ARTICLE

How the nature and charge of metal cations affect vibrations in acetone solvent molecules

Received 00th January 20xx,
Accepted 00th January 20xx

DOI: 10.1039/x0xx00000x

Apakorn Phasuk,[a] Joel Lemaire,[b] Vincent Steinmetz,[b] Philippe Maître [b] and Ricardo B. Metz*[a]

Vibrational spectra of a series of gas-phase metal 1+ and 2+ ions solvated by acetone molecules are collected to investigate how the metal charge, number of solvent molecules and nature of the metal affect the acetone. The spectra of $Cu^+(Ace)(N_2)_2$, $Cu^+(Ace)_4$, and $M^{2+}(Ace)_4$, where M = Co, Ni, Cu, and Zn are measured via photodissociation by monitoring fragment ion signal as a function of IR wavenumber. The spectra show a red shift of the C=O stretch and a blue shift of the CC antisymmetric stretch. DFT calculations are carried out to provide the simulated spectra of possible isomers to be compared with the observed vibrational spectra, and specific structures are proposed. The red shift of the C=O stretch increases as the number of acetone molecules decreases. Higher charge on the metal leads to a larger red shift in the C=O stretch. Although all of the M^{2+} complexes have very similar red shifts, they are predicted to have different geometries due to their different electron configurations. Unexpectedly, we find that the calculated red shift in the C=O stretch in $M^{+/2+}(Ace)$ is highly linearly correlated with the ionization energy of the metal for a wide range of metal cations and dications.

Introduction

Solvents can affect reaction rates, product yield and selectivity by changing energy barriers, competing with other substrates, inhibiting undesired reactions or altering the structure and stability of intermediates and substrates, and even directly participating in the reaction.[1–3] Studies of solute-solvent interactions usually focus on the short-range interaction between a solute and solvent molecules in its immediate environment, especially the first solvation shell that dominates the energetics of solvation.[4] For simple metal ions M^+ and M^{2+}, the first-shell solvent molecules donate electron density to the ion, stabilizing the charge. This Interaction can also affect structure and bonding of the solvent. Acetone is a common organic solvent and the carbonyl functional group also plays a crucial role in biological systems such as proteins and enzymes.[5–10]

Unfortunately, in the condensed phase it is difficult to characterize solvation at the molecular level due to the complexity of the environment and the lack of control one has over the solvent coordination. In contrast, studies of gas-phase cluster ions allow researchers to investigate metal-ligand interactions with well-defined stoichiometry and in the absence of perturbing interactions with the environment. They also provide an opportunity to study thermodynamics, structure, coordination and reactions by combining highly sensitive and selective characterization techniques with detailed calculations.[11]

Thus, gas-phase metal ion–acetone complexes involving Li^+, Na^+, Al^+, ScO^+, Ti^+, Fe^+, $Co^{+/2+}$, $Cu^{+/2+}$, $Ag^{+/2+}$, Ca^{2+}, Mn^{2+}, Ni^{2+}, Zn^{2+} and UO_2^{2+} have been studied in the gas phase using various mass-based techniques including collision-induced dissociation (CID),[12–16] Fourier transform ion cyclotron resonance (FT-ICR),[17] FT-ICR coupled with radiative association (RA),[18] high-pressure mass spectrometry (HPMS),[19] and reflectron time-of-flight mass spectrometer (RTOFMS).[20,21] Although studies using mass spectrometry can reveal cluster dissociation energies and pathways and the relationship between cluster composition and reactivity, they don't directly provide information on structure and bonding. This structural information can be obtained using vibrational spectroscopy in concert with quantum chemistry calculations.[22] Vibrational spectroscopy has been used to characterize a few $M^{+/2+}$-acetone complexes. Velasquez et al.[23] investigated the effect of the metal on the C=O stretch frequency in M^+–acetone complexes (M = Mg, Al, Ca) by measuring spectra from 1550 to 1850 cm^{-1}. Groenewold et al. examined how the interaction between UO_2^{2+} and acetone affects vibrational frequencies in the uranyl and ligand.[24] They found that the frequency shifts decrease as the number of ligands increases. Subsequently, they observed similar results in clusters of $[CeOH]^{2+}$ with three and four acetones.[25] Recently, we studied complexes of Al^+ and acetone and discovered that addition of the fifth acetone ligand leads to a reductive C–C coupling reaction, producing a pinacolate.[26] However, a broad

[a] Department of Chemistry, University of Massachusetts Amherst, Amherst, MA 01003, USA. E-mail: rbmetz@chem.umass.edu
[b] Laboratoire de Chimie Physique, Université de Paris XI, Orsay, France. E-mail: philippe.maitre@u-psud.fr

† Electronic Supplementary Information (ESI) available: Mass spectrum; difference mass spectrum; experimental and calculated vibrational spectra; correlation of red shift in C=O stretch frequency of $M^+(Ace)$ with various properties); calculated energies, geometries, vibrational frequencies and intensities. See DOI: 10.1039/x0xx00000x

understanding of how metal type and charge and the number of ligands affects the bonds in the acetone is still lacking.

In this work, the interactions of Cu^+, Co^{2+}, Ni^{2+}, Cu^{2+} and Zn^{2+} with acetone are studied in the gas phase using photodissociation vibrational spectroscopy of ion-acetone complexes. The spectra reveal information about the structures of the ions and the covalent bonds in the complexes. We investigate how the nature of the metal, the charge on the ion, and the number of acetone molecules influence the perturbation of bonds in the acetone. These fundamental studies will help our understanding of metal ion solvation.

Experimental and computational methods

Experiments on singly-charged ions were carried out in the Metz lab, those on dications were performed at the Centre Laser Infrarouge d'Orsay (CLIO) free electron laser facility. The $Cu^+(Ace)(N_2)_2$ and $Cu^+(Ace)_4$ (Ace = acetone) complexes are produced using a home-built dual time–of–flight mass spectrometer[27] by ablating a metal rod with a Nd:YAG (532 nm) laser and pulsing acetone seeded in helium over the resulting metal ions. The gas mixture consists of 0.08 to 0.25% acetone/10 to 20% N_2/80 to 90% He at a backing pressure of 20 psi. The ions then undergo a supersonic expansion and cool to a rotational temperature of ~15K.[28] They are then extracted into a reflectron time-of-flight mass spectrometer. At the turning point of the reflectron, the mass-selected ions are irradiated with a pulsed, tunable IR laser. A Nd:YAG-pumped (1064 nm) OPO/OPA IR laser system (LaserVision) coupled to a $AgGaSe_2$ crystal is used to generate light from 1100 to 2000 cm^{-1}. The power is 0.25 mJ/pulse near 2000 cm^{-1}, with a line width of ~2 cm^{-1}. The dissociation is increased by multipassing the IR laser beam through the cluster about 10 times using two curved mirrors.[29] The wavelength is calibrated using the methane absorption spectrum.[30] The vibrational spectrum of the ions is measured by monitoring fragment ion signal as a function of IR wavenumber and normalizing to parent signal and laser fluence.

Spectra of $M^{2+}(acetone)_4$ complexes were measured at the CLIO free electron laser facility. The setup used for these experiments has been described in detail.[31–33] The ions of interest are produced by electrospray of solutions of MCl_2 (M=Co, Ni, Cu, Zn) salts dissolved in acetone and are collected in a modified Bruker Esquire 3000+ Paul-type ion trap. Spectra are measured by monitoring signal due to fragment ions while scanning the IR wavelength. The CLIO IR-FEL[34] is based on a 10 to 50 MeV electron accelerator. To cover the 1000-2000 cm^{-1} region, the electron energy was set to 43 MeV and the photon energy is scanned by adjusting the gap in an undulator in the optical cavity. The IR light emitted by the FEL consists of 8 µs long macropulses at a repetition rate of 25 Hz. Each macropulse contains ~500 micropulses, each a few picoseconds long and separated by 16 ns. The average IR power in these studies was ~750 mW, which corresponds to micropulse and macropulse energies of ~60 µJ and ~30 mJ, respectively.

The calculations are performed with the Gaussian09 program package[35] using the B3LYP+D3[36]/6–311+G(d,p) and ωB97X-D[37]/6–311+G(d,p) level of theory to determine isomeric structures, optimized geometries and harmonic vibrational spectra. The harmonic vibrational frequencies are multiplied by 0.99 based on the best value appropriate for these metal cation-acetone complexes. For Cu^+ complexes, anharmonic vibrational frequencies were also calculated using B3LYP+D3/6–311+G(d,p) and are not scaled. The zero-point energies are included in all reported energies. Simulated spectra are calculated by convoluting the calculated stick spectrum with a Gaussian with 20 cm^{-1} fwhm. Natural bond orbital (NBO) analysis[38] and calculations of atomic volume were carried out using Gaussian09, with the Def2-TZVP basis set and effective core potential for elements with Z≥37.

Results and discussion

$M^{2+}(Ace)_4$ complexes (M=Co, Ni, Cu, and Zn)

The calculated bond dissociation energies (BDE) for loss of acetone (Table 1) from $M^{2+}(Ace)_4$ (M = Co, Ni, Cu, Zn) are at least 174 kJ/mol (14550 cm^{-1}). The dissociation is due to IRMPD, which is facilitated by the high fluence and temporal profile of the CLIO IR beam. The major product ions observed are $H^+(acetone)$ and $MOH^+(acetone)_2$. They are likely formed by loss of acetone, followed by reaction with a small amount of residual water in the ion trap:

$$M^{2+}(acetone)_4 + n\ h\nu \rightarrow M^{2+}(acetone)_3 + acetone$$

$$M^{2+}(acetone)_3 + H_2O \rightarrow [M^{2+}(acetone)_3(H_2O)]^* \rightarrow MOH^+(acetone)_2 + H^+(acetone)$$

The dissociation pathways of $M^{2+}(Ace)_n$ have been studied using high-energy, single-collision collision-induced dissociation (CID) and UV photodissociation. Duncombe et al.[16] observed three pathways in CID of $Zn^{2+}(Ace)_4$: charge transfer (loss of Ace^+), C-O cleavage upon ZnO^+ formation, and neutral ligand loss. Subsequently, Wu et al.[13] investigated CID of $M^{2+}(Ace)_n$, n ≤ 6, complexes for M = Ca, Mn, Co, Ni, and Cu. They found that for metals with a low 2nd ionization energy (IE) (e.g., Ca) the major pathway is loss of neutral ethylene, while charge transfer dominates for metals with high 2nd IE (Ni and Cu). Metals with intermediate 2nd IE (Mn and Co) dissociate via multiple pathways, including loss of neutral ethylene, charge transfer, loss of H^+L upon inter-ligand H^+ transfer, loss of $(L - H)^+$ upon H^- transfer, and loss of CH_3CO^+. They also calculated the sequential BDE of $M^{2+}(Ace)_n$ complexes using B3LYP/6–311+G**. Puskar and Stace studied photofragmentation of $Cu^{2+}(Ace)_n$, n = 4–8 in the UV, at 266 and 280 nm.[39] For n = 4, they found that the only fragment is $Cu^+(Ace)_2$, corresponding to the loss of one neutral and one charged acetone. The higher energies in these studies leads to a much richer range of products than is observed in our work, in which the sequential nature of IRMPD results in near-threshold dissociation and simple ligand loss.

ARTICLE

Table 1 Calculated and Experimental Binding Energies of $Cu^+(Ace)(N_2)$, $Cu^+(Ace)(N_2)_2$, $Cu^+(Ace)_n$ and $M^{2+}(Ace)_4$, n = 1 and 4, M = Co, Ni, Cu, and Zn.

Species	B3LYP+D3/6–311+G(d,p)		ωB97X-D/6–311+G(d,p)	
	cm^{-1}	kJ/mol	cm^{-1}	kJ/mol
Cu^+ – Ace	19289 16600±400	230.8 198.6±4.3[a] 203.0[b]	18355	219.6 192.4[c]
$Cu^+(Ace)$ – N_2	8749	104.7	8252	98.7
$Cu^+(Ace)(N_2)$ – N_2	1573	18.8	1563	18.7
$Cu^+(Ace)$ – Ace	17357	207.6 209.8±6.5[a] 194.6[b]	17029	203.7 204.9[c]
$Cu^+(Ace)_2$ – Ace	6073	72.6 64.3±2.4[a] 62.6[b]	6260	74.9 69.4[c]
$Cu^+(Ace)_3$ – Ace	5484	65.6 61.0±5.4[a] 37.2[b]	5494	65.7 63.4[c]
$Co^{2+}(Ace)_3$ – Ace	16832	201.4	17150	205.2
$Ni^{2+}(Ace)_3$ – Ace	16122	192.9	16560	198.1
$Cu^{2+}(Ace)_3$ – Ace	14550	174.1	15171	181.5
$Zn^{2+}(Ace)_3$ – Ace	15973	191.1	16295	194.9

Calculations include zero point energy and are at zero Kelvin. [a] experimental value, threshold collision-induced dissociation at 0 K.[40] [b] B3LYP/6–31+G(2d,2p) using B3LYP/6–31G* optimized geometries.[40] [c] MP2(full)/6–311+G(2d,2p) level of theory using the B3LYP/6–31G* optimized geometries.[40]

Table 2 Calculated (with Scaling Factor = 0.99) and Experimental Vibrational Frequencies of M^+ and M^{2+} – Acetone Complexes, M = Al, Co, Ni, Cu, and Zn.

Species	Experiment			B3LYP+D3 Calculation			ωB97X-D Calculation		
	$\nu_{C=O}$ stretch	ν_{CH3} deform	ν_{CC} stretch	$\nu_{C=O}$ stretch	ν_{CH3} deform	ν_{CC} stretch	$\nu_{C=O}$ stretch	ν_{CH3} deform	ν_{CC} stretch
Acetone	1731 VS	1454 S 1435 S 1410 S 1364 VS	1216 VS	1769 S	1472 1456 1374 M	1220 M	1817 S	1476 1460 1452 1385 M 1376	1234
$Co^{2+}(Ace)_4$	1645 VS 1618	1440 1408 1388 M	1269	1639 VS 1634 VS 1630 VS	1452 1422 1385 M 1374 M	1278	1719 1690 VS 1685 VS 1680 VS	1457 1426 1401 M 1382	1287
$Ni^{2+}(Ace)_4$	1645 VS 1632	1435 1421 1408 1388 M	1270	1641 VS 1638 VS 1635 S	1455 1421 1384 M	1277	1692 VS 1689 VS 1686 S	1456 1430 1400 M 1382	1286
$Cu^{2+}(Ace)_4$	1659 1632 VS	1446 1426 1386 M	1272	1648 VS 1638 VS	1472 1455 1423 1384 M 1373 M	1274	1698 VS 1689 VS	1475 1458 M 1428 1399 1382 M	1285
$Zn^{2+}(Ace)_4$	1638 VS 1624	1426 1406 1386 M 1373	1260	1639 VS 1636 VS 1633 VS	1452 1420 1386 M 1374 M	1278	1691 VS 1689 VS 1683 VS	1458 1425 1400 M 1382	1287

$Cu^{+}(Ace)_4$	1704 VS	1435 1391	1265	1712 M 1700 S 1697 S 1693 S	1476 1458 1443 1389 M 1382 1379 M	1255 1246	1769 M 1754 S 1751 S 1748 S	1479 1461 1447 1401 M 1398 M 1389 M	1264 1259
$Cu^{+}(Ace)(N_2)_2$	1679 VS 1640	1428 VS 1378 VS	1272 S	1682 S	1473 1452 1430 1388 M 1379	1266	1736 S	1470 1458 1435 1401 M 1385	1275
$Cu^{+}(Ace)(N_2)$	N/A	N/A	N/A	1659 S	1464 1453 1425 1387 M 1377	1273	1715 S	1470 1458 1430 1401 M 1383	1282
$Cu^{+}(Ace)$	N/A	N/A	N/A	1649 S	1463 1453 1423 1386 M 1375	1270	1709 S	1470 1458 1430 1400 M 1383	1280
$Al^{+}(Ace)(N_2)^{a}$	1627 VS	1469 1450 1421 1392 1369	1295	1621 VS	1466 1450 1415 M 1382 M 1369	1278	1669 VS	1472 1455 1423 M 1396 M 1377	1288

Calculations performed at zero Kelvin with the 6–311+G(d,p) basis set unless indicated otherwise. [a] Experimental value at 0 K, B3LYP+D3/6–311+G(d,p) and ωB97X-D/6–311+G(d,p).[26]

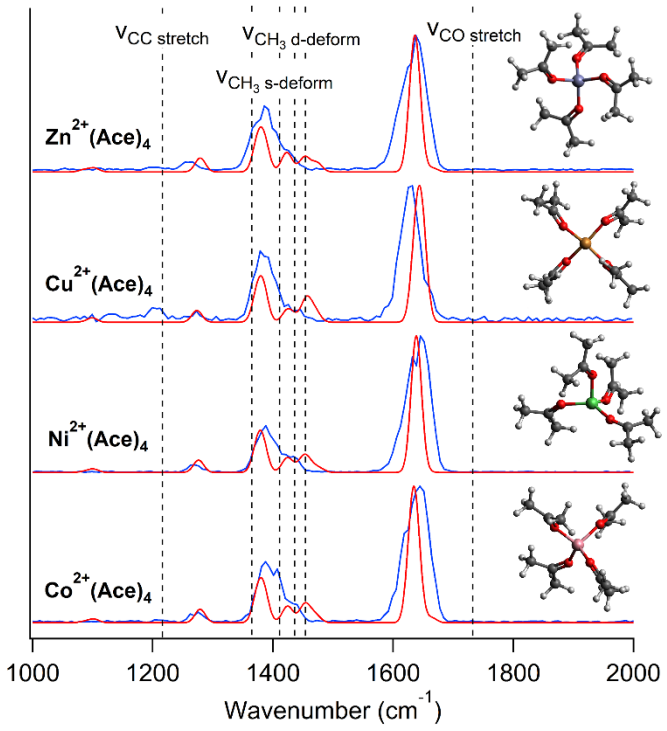

Figure 1 Vibrational spectra of $M^{2+}(Ace)_4$, from 1000 to 2000 cm^{-1} (blue); simulated harmonic spectra of the lowest-lying isomer and optimized geometries of $M^{2+}(Ace)_4$, where M = Co, Ni, Cu, and Zn, at the B3LYP+D3/6-311+G(d,p) level with scaling factor = 0.99 (red). The y-axis is normalized photofragment yield (experiment) at the C=O stretch frequency and absorption cross section (simulations). The experimental positions of the antisymmetric CC stretch, CH_3 deformations and C=O stretch in bare acetone are indicated by dashed vertical lines.

The experimental and calculated spectra of $M^{2+}(Ace)_4$ are shown in Fig. 1 and the peak positions are listed in Table 2. All $M^{2+}(Ace)_4$ experimental spectra are very similar in both peak positions and intensities. The spectra are dominated by an intense peak near 1640 cm^{-1} assigned to the C=O stretch. This is red shifted from its position in isolated acetone (1731 cm^{-1}). There is a group of overlapping medium-intensity peaks observed near 1400 cm^{-1}. They correspond to various bends of the methyl groups: the CH_3 degenerate deformations (~1410-1450 cm^{-1} in acetone) and CH_3 symmetric deformation (~1360 cm^{-1} in acetone). Binding to the metal only leads to very small shifts in these vibrations. There is also a weak peak near 1270 cm^{-1}. This corresponds to the antisymmetric CC stretch and is substantially blue-shifted from its position at 1216 cm^{-1} in acetone. The spectra are very similar. To emphasize the different shifts for each metal, the experimental spectra are overlaid in Fig. 2. $Cu^{2+}(Ace)_4$ shows the largest red shift in the C=O stretch (to 1632 cm^{-1}), followed by $Zn^{2+}(Ace)_4$ (1638 cm^{-1}) and, equally, $Co^{2+}(Ace)_4$ and $Ni^{2+}(Ace)_4$ (1645 cm^{-1}). $Zn^{2+}(Ace)_4$ has a slightly smaller blue shifted for the CC stretch (1260 cm^{-1}) than the other metals (1269-1272 cm^{-1}). The calculated spectra match well with the experimental spectra. The calculated geometries and vibrational frequencies of $M^{2+}(Ace)_4$ and all other species discussed in this paper are in Table S1 (B3LYP+D3) and S2 (ωB97X–D). Overall, although the geometries and bond dissociation energies are very similar, the calculated vibrational spectra using the B3LYP+D3 functional provide a better match to experiment than those with the ωB97X–D functional, so the

discussion will focus on the B3LYP+D3 results. The calculations predict that, as expected, in $M^{2+/+}(Ace)_n$, n = 1 and 4 the ligands are generally arranged at maximum inter-ligand distance. The M–O bond lengths increase as the number of ligands increases due to metal–ligand interaction weakening and decreases as charge increases due to the metal–ligand interaction getting stronger. The acetone binds to $M^{2+/+}$ using the O atom. If bonding is purely electrostatic then the cation interacts with the dipole moment of acetone and M-$\widehat{O}$-C is linear. If the cation interacts strongly with the lone-pair p electrons on the oxygen via charge transfer, then the the M-$\widehat{O}$-C is, in the limiting case, 90°.[41,42] In addition, Bauschlicher and co-workers[43] pointed out that transition metals have the ability to reduce ligand repulsion by sdσ hybridization, reducing the charge density on the σ axis. This is most important for complexes with one and two ligands. Due to symmetry, sdσ hybridization does not occur for tetrahedral complexes, but it can occur for other geometries.

The $M^{2+}(Ace)_4$ complexes will be discussed in the order of the complexity of their electronic structure: Zn, Ni, Co, Cu. As expected for a four-coordinate d^{10} complex, computed $Zn^{2+}(Ace)_4$ has an approximately tetrahedral structure. The bond angles O_1–$\widehat{Zn}$–O_3 and O_2–$\widehat{Zn}$–O_4 are 112.5° and 107.4° respectively (see details in Table S3). Because of charge transfer, the Zn–$\widehat{O}$–C are bent: 134.0 to 139.3°. This agrees with previous work. Unlike Mg^{2+}(Ace), Ca^{2+}(Ace) and $Zn^{2+}(H_2O)$, Peschke *et al*.[44] found that the Zn-$\widehat{O}$-C in Zn^{2+}(Ace) is bent instead of being linear because the increase in charge transfer (compared to the other molecules they studied) leads to better alignment of the empty sdσ orbital on Zn^{2+} with the lone pair electrons on oxygen. El-Nahas investigated the thermodynamic and/or kinetic stabilities of Be, Mg, Ca, and Zn dications with formaldehyde, acetone, and DMSO.[41] He also calculated bent Zn-$\widehat{O}$-C in Zn^{2+}(Ace) due to substantial charge transfer between Zn^{2+} and oxygen in acetone, which was not found in the other metals in his work. For $Zn^{2+}(Ace)_4$, our calculations predict that the C=O bond lengthens from 1.214 Å in bare acetone to 1.247 - 1.250 Å in the complex, whereas r_{C-C} shortens from 1.520 Å to 1.487 - 1.492 Å. These results are consistent with the experimental and calculated vibrational spectra which show a red shift in the C=O stretch due to bond weakening and blue shift in the antisymmetric C-C stretch due to bond strengthening. The calculated r_{Zn-O} is 1.978 - 1.987 Å, while the computed bond dissociation energy (BDE) to lose acetone is 191.1 kJ/mol.

The Ni^{2+} atom has a triplet (d^8) ground state. The singlet (also d^8) is 14032 cm^{-1} higher in energy. So, complexes of Ni(II) are expected to be high spin (triplet) for weakly interacting ligands and low spin (singlet) for strongly interacting ligands. We calculated both triplet and singlet states of $Ni^{2+}(Ace)_4$. The triplet is predicted to be lower in energy with a distorted tetrahedral geometry, while the singlet has the expected square planar geometry, but is 2093 cm^{-1} higher in energy. So, our conclusion is that acetone is not a sufficiently strong-field ligand to favor a low-spin ground state. For the triplet, we also carried out constrained geometry optimizations with a square planar geometry, but it relaxes to the distorted tetrahedral minimum when the constraints are lifted.

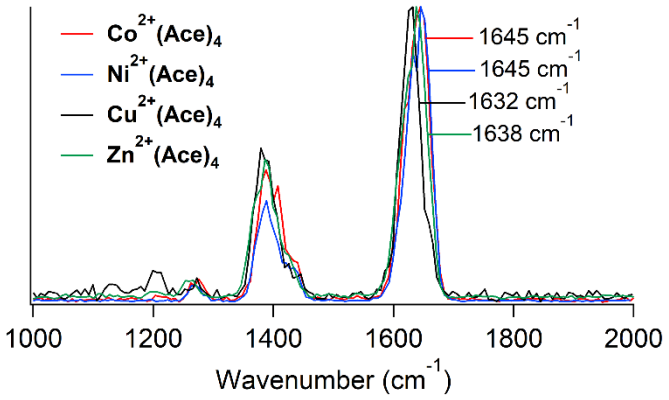

Figure 2 Overlaid vibrational spectra of $M^{2+}(Ace)_4$ from 1000 to 2000 cm^{-1}. The y-axis is normalized photofragment yield at the C=O stretch frequency.

Unfortunately, the experimental spectrum can't distinguish between the high- and low-spin complexes, as the vibrational spectrum in the region we study is not sensitive to the relative orientation of the ligands in space, but rather to how interaction with the metal affects the bonds in each acetone. This is demonstrated in Figure S1, which shows that the simulated vibrational spectra of low- and high-spin $Ni^{2+}(Ace)_4$ are nearly identical from 550-3200 cm^{-1} and have minor differences from 200-550 cm^{-1}.

Our calculations predict that triplet $Ni^{2+}(Ace)_4$ has a distorted tetrahedral structure. The O_1–$\widehat{Ni}$–O_3 and O_2–$\widehat{Ni}$–O_4 angles are 138.5° and 107.4°. The M-$\widehat{O}$-C is bent, with Ni–$\widehat{O}$–C ranging from 131.7° to 144.8°. There is a larger variation in the bond length between the metal ion and oxygen atoms than in the other $M^{2+}(Ace)_4$, with r_{Ni-O} = 1.949 to 1.975 Å. The BDE is calculated to be 192.7 kJ/mol. The bond lengths in the ligand in $Ni^{2+}(Ace)_4$ are close to those in other $M^{2+}(Ace)_4$, with $r_{C=O}$ = 1.245 to 1.247 Å and r_{C-C} = 1.487 to 1.493 Å, consistent with the similarity of the vibrational spectra.

The calculations predict that the d^7 complex $Co^{2+}(Ace)_4$ has a slightly distorted tetrahedral structure with O_1–$\widehat{Co}$–O_3 and O_2–$\widehat{Co}$–O_4 113.7° and 109° respectively. The Co-O bond lengths range from 1.970 to 1.979 Å and the calculated BDE is 201.4 kJ/mol. As with the other $M^{2+}(Ace)_4$, the Co–$\widehat{O}$–C are bent (135.9° to 141.2°). The ligand geometries are also similar to those of the other complexes, with $r_{C=O}$ = 1.245 to 1.249 Å and r_{C-C} = 1.487 to 1.492 Å.

For $Cu^{2+}(Ace)_4$, the calculation predicts a square planar geometry, which is typical of four-coordinate Cu(II) complexes.[45–47] The bond angles of both O_1–$\widehat{Cu}$–O_3 and O_2–$\widehat{Cu}$–O_4 are 180.0°. The oxygen in acetone binds to Cu^{2+} with bent alignment, Cu–$\widehat{O}$–C = 134.3 to 135.4°. The calculated bond lengths are $r_{C=O}$ = 1.243 to 1.245 Å, r_{C-C} = 1.490 to 1.493 Å, and r_{Cu-O} = 1.964 to 1.969 Å, which is similar to the values in the other $M^{2+}(Ace)_4$ complexes. The BDE is calculated to be 174.1 kJ/mol which is slightly lower than for the other dication

complexes. The computed BDE of $Cu^{2+}(Ace)_4$ is significantly larger than $Ag^{2+}(Ace)_4$ (~130 kJ/mol)[48] due to stability that can be explained with hard and soft acids and bases theory (HSAB). Cu^{2+} is a harder acid than Ag^{2+}, so Cu^{2+} binds more strongly to the acetone oxygen (a hard base).

The vibrational spectra of acetone-solvated dications have been measured by Groenewold *et al*. They measured[24] the spectra of $UO_2^{2+}(Ace)_n$ (n = 2-4). For n = 4, the C=O stretch is observed at 1630 cm^{-1}. This red shift is slightly larger than we observe in our M^{2+} complexes, potentially due to the higher oxidation state on the uranium metal center (+4). The antisymmetric CC stretch of $UO_2^{2+}(Ace)_4$ is observed at 1249 cm^{-1}, which is blue shifted from bare acetone (1216 cm^{-1}), however the blue shift is smaller than we observe for $M^{2+}(Ace)_4$, ~1270 cm^{-1}. They also studied complexes of $[CeOH]^{2+}$ with three and four acetones.[25] For $(CeOH)^{2+}(Ace)_4$, the C=O stretch was observed at 1650 cm^{-1} and CC stretch at 1247 cm^{-1}. These shifts are smaller than those in $UO_2^{2+}(Ace)_4$ and $M^{2+}(Ace)_4$.

$Cu^+(Ace)(N_2)_2$

A typical mass spectrum obtained when ablating copper with acetone/N_2/He is shown in Figure S2. The relative peak intensities depend on the concentration of acetone in the gas mixture, with larger clusters dominating at higher concentration. No magic numbers are observed for $Cu^+(Ace)_n$. The Cu^+ - Ace BDE has been measured[40] to be 16600±400 cm^{-1} and is calculated to be slightly higher (Table 1), so it is not surprising that we do not observe photofragmentation at the ~0.25 mJ laser power in the Metz lab. This is also the case for $Cu^+(Ace)(N_2)$, where loss of N_2 is calculated to require >8000 cm^{-1}. The BDE of $Cu^+(Ace)(N_2)_2$ is computed to be only ~1570 cm^{-1}, and it dissociates readily. Figure S3 shows the mass spectrum and laser on – laser off difference mass spectrum obtained for $Cu^+(Ace)(N_2)_2$, showing loss of N_2. Although the BDE of $Cu^+(Ace)_4$ is calculated to be ~5500 cm^{-1}, it dissociates readily, via loss of one acetone. This is likely due to multi-passing of the IR beam facilitating IRMPD. Previously, the photodissociation pathways of $Cu^+(Ace)_n$, n = 1–6, were investigated using UV photofragmentation at 266 and 280 nm by Puskar and Stace.[39] They found that the dominant fragment is $Cu^+(Ace)(CO)$ for n = 2 and neutral ligand loss for n ≥ 3. Their observation is in good agreement with our results, in which the loss of a neutral acetone is measured for n = 4.

Figure 3 shows the IR vibrational spectrum of $Cu^+(Ace)(N_2)_2$ measured by monitoring N_2 loss and the simulated scaled harmonic (red) and unscaled anharmonic (black) vibrational spectra of $Cu^+(Ace)(N_2)_k$, k = 0–2. The largest peak in the experimental spectrum is the C=O stretch, at 1679 cm^{-1}, which is red shifted compared to isolated acetone (1731 cm^{-1}).[49] The CH_3 degenerate-deformation and CH_3 symmetric-deformation are observed at 1428 cm^{-1} and 1378 cm^{-1}. Meanwhile, the CC stretch blue shifts from 1216 cm^{-1} to 1272 cm^{-1}. The simulated harmonic calculation matches most of the peak positions quite well, except that the intensity ratio between the bends and the

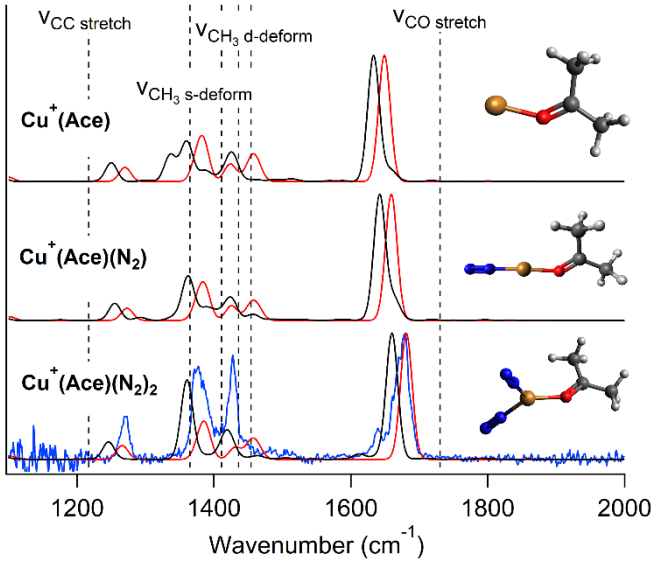

Figure 3 Vibrational spectrum of $Cu^+(Ace)(N_2)_2$ in the 1100-2000 cm^{-1} region (blue) and simulated harmonic, scaling factor 0.99 (red) and unscaled anharmonic (black) spectra of the lowest-lying isomer of $Cu^+(Ace)(N_2)_k$, k=0–2, at the B3LYP+D3/6-311+G(d,p) level. The antisymmetric CC stretch, CH_3 bends and C=O stretch in bare acetone are represented by dashed vertical lines. The y-axis is normalized photofragment yield (experiments) at the C=O stretch frequency and relative absorption cross section (simulations).

C=O stretch is too small. The calculation is also missing the small peak observed at 1640 cm^{-1}. As a consequence, we decided to perform anharmonic calculations, and the result is in excellent agreement with experiment, except that the frequencies are consistently approximately 20 cm^{-1} too low. The relative intensities are better reproduced, and the simulation predicts a small peak at 1612 cm^{-1}. This is due to the overtone of the symmetric CC stretch and corresponds to the 1640 cm^{-1} peak in the experiment. Velasquez *et al*. also observed this overtone in $Mg^+(Ace)(Ar)$ (1653 cm^{-1}) and $Ca^+(Ace)(Ar)$ (1643 cm^{-1}) and noted that it gains intensity due to Fermi resonance with the nearby C=O stretch.[23]

Figure 3 also shows how the N_2 tags affect the calculated spectra. They slightly perturb the calculated geometry of $Cu^+(Ace)$ with $r_{C=O}$ shifting from 1.237 to 1.234 Å and r_{Cu-O} extending from 1.890 to 1.945 Å with the addition of two N_2. The computed vibrational frequencies also shift slightly, with the largest shift (33 cm^{-1}) in the C=O stretch. The larger the number of N_2 tags, the smaller the frequency shifts (compared to isolated acetone), due to the N_2 donating electron density to the metal, reducing its effective charge.

Chu *et al*.[40] studied the CID of $Cu^+(Ace)_n$, n = 1–4, with Xe. They found that the BDE of $Cu^+(Ace)$ is 198.6±4.3 kJ/mol. They calculated 203.0 kJ/mol at the B3LYP/6–31+G(2d,2p) level, which is slightly lower than our calculated BDE due to our use of a larger basis set and inclusion of dispersion. Overall, the agreement between their measured BDEs for $Cu^+(Ace)_n$, n = 1–4 and our calculations is excellent (Table 1). The spectrum of $Al^+(Ace)(N_2)$ from our previous work[26] is also provided in Figure 4. With the same charge and number of acetones, the

experimental and computed C=O stretch of $Al^+(Ace)(N_2)$ shows a much larger red shift than $Cu^+(Ace)(N_2)_2$. This is somewhat surprising, as the measured Al^+-Ace BDE is only 177 kJ/mol.[50] Note that the measured spectra of the $M^{2+}(Ace)_4$ complexes are broader than those of the singly-charged ions. This is primarily due to the use of much higher laser fluences available at CLIO, and required to photodissociate the strongly-bound dication complexes.

The observed red shifts vary widely, and cannot be explained by the BDE's of the complexes. One possibility is that the red shifts strongly depend on the M-O-C angle, which is calculated to be 180° in $Al^+(Ace)$ and 140° in $Cu^+(Ace)$. However, constraining Al–$\widehat{O}$–C to 140° increases the red shift by only 5 cm^{-1}, while forcing the Cu complex to be linear slightly reduces the red shift. So, we looked for other possibilities. In their study of $M^+(Ace)$ (M=Mg, Ca, Al), Velasquez *et al*.[23] suggested that the larger red shift observed for Al^+ is due to its small size. Subsequently, Zhang *et al*.[51] caried out natural bond order (NBO) analysis of DFT calculations of metal-acetone complexes of Li^+, Na^+, K^+, Rb^+, Cs^+, Mg^+, Ca^+, Al^+, Mg^{2+} and Ca^{2+}. They attributed the extent of the red shift to the change in population (compared to isolated acetone) of the σ*(CO) and π*(CO) natural orbitals rather than to the ion size.

We investigated how the DFT-calculated red shifts in a wide range of $M^+(Ace)$ and $M^{2+}(Ace)$ complexes depend on various properties of the metal cations and of the complexes (Table S4). Figure S4 shows that there is little overall correlation between the computed carbonyl red shift in $M^+(Ace)$ and the ionic radius of M^+ (there is even less correlation if M^{2+} are included). For a particular group, the red shift decreases slightly with increasing ionic radius. There are many ways to determine ionic radii. We have used the approach of Rahm *et al*.[52] who define it based on the volume in which the electron density is at least 0.001 electrons per cubic bohr, from calculations on the ion. This has the advantages that it relies on properties of the isolated ion, rather than ions in a crystal lattice, and can be readily calculated for any element in any charge state. Figure S5 shows the relationships between the computed carbonyl red shift and changes in populations in antibonding orbitals Δσ*(CO) and Δπ*(CO). As noted by Zhang *et al*.[51] there is a strong correlation with both, with an increase in antibonding orbital occupation proportional to an increased red shift. However, the change in orbital populations is a property of the metal-acetone complex, rather than an intrinsic property of the metal. So, we sought an answer to the more fundamental question of which properties of the metal cation determine the extent of the red shift in the acetone C=O stretch, seeking a correlation with a property of the isolated metal ion.

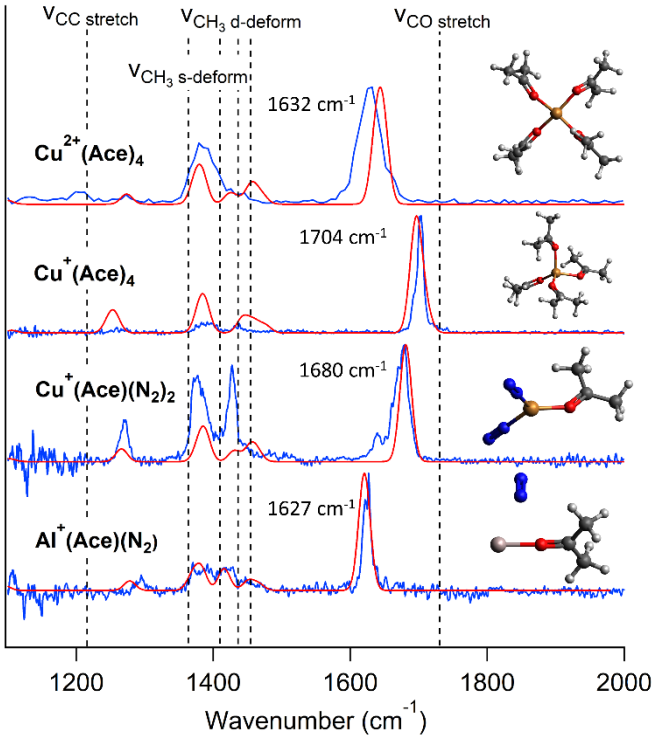

Figure 4 Vibrational spectra of $Al^+(Ace)(N_2)$,[26] $Cu^+(Ace)(N_2)_2$, $Cu^+(Ace)_4$ and $Cu^{2+}(Ace)_4$ (blue), in the region 1100-2000 cm^{-1}. Simulated spectra of the lowest-lying isomer of each ion at the B3LYP+D3/6-311+G(d,p) level with scaling factor = 0.99 (red). The CC stretch, CH_3 deformation and C=O stretch in bare acetone are represented by dashed vertical lines. The y-axis is normalized photofragment yield (experiments) at the C=O stretch frequency and relative absorption cross section (simulations).

In a very recent paper, Duda and Dixon[53] observed a clear linear correlation between the BDE of closed-shell metal cation-triphenylphosphine complexes and the hardness, η, of the ion, which for M^+ corresponds to

$\eta = {}^1/_2\,(2^{nd}\ IE - 1^{st}\ IE)$

There are different correlations for group 1 and 11 cations and for group 2 dications. There is modest linear correlation between the calculated red shifts and hardness (Fig. S6), but there are different series, with different slopes, for ions in each group.

There is a much more general correlation: as shown in Figure 5, the computed carbonyl red shifts have an excellent correlation with the ionization energy (IE) of the metal. This holds for

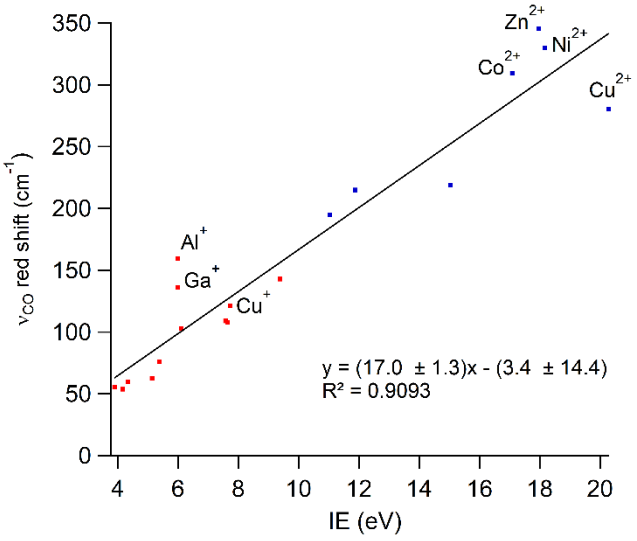

Figure 5 Correlation of calculated red shift in C=O stretch frequency in $M^{+/2+}(Ace)$ with metal ionization energy. Singly charged ions are in red and doubly charged ions are in blue.

M^+(Ace) and M^{2+}(Ace) complexes (in the latter case, the relevant quantity is the second IE), and for a wide variety of metals. We did not include metal ions that react with acetone. As the IE of acetone is 9.703 eV, many of the M^{2+}(Ace) are metastable with respect to $M^+ + Ace^+$. However, the correlation still holds, although Cu^{2+} (IE = 20.29 eV) is a slight outlier. This is probably the upper limit of IE, as the calculated Ag^{2+} (IE = 21.49 eV) complex spontaneously dissociates to $Ag^+ + Ace^+$. Al^+ and, to a lesser extent, Ga^+ have larger red shifts than is expected based on their IE's. The results show that the IE has a strong correlation with the carbonyl red shift, even stronger than the correlation with the calculated (NBO) charge on the acetone in the complex. This implies that there is a strong electrostatic component to the red shift.

$Cu^+(Ace)_4$

The infrared dissociation spectrum of $Cu^+(Ace)_4$ is shown in Figure 4. The spectrum consists of an intense C=O stretch at 1704 cm^{-1}, CH_3 deformations at 1435 cm^{-1} and 1391 cm^{-1}, and a very weak CC antisymmetric stretch at 1265 cm^{-1} (this region of the spectrum is magnified in Fig. S7). As shown in Fig. 4, the C=O stretch is significantly less red-shifted from isolated acetone compared to $Cu^{2+}(Ace)_4$ and $Cu^+(Ace)(N_2)_2$, which have the same number of ligands and the same positive charge, respectively. A decrease in charge or increase in the number of ligands reduces the interaction between a metal ion and the acetone ligands, which leads to a substantially smaller red shift in the C=O stretch. The BDE is calculated to be 65.6 kJ/mol, which matches well with the experiment of Chu *et al*.[40] (61.0±5.4 kJ/mol) and is substantially less than for $Cu^{2+}(Ace)_4$ and Cu^+(Ace). While $Cu^{2+}(Ace)_4$ is calculated to have a square planar geometry, in $Cu^+(Ace)_4$ the calculations predict that the acetones bind to Cu^+ in a distorted tetrahedral geometry, with Cu-$\widehat{O}$-C angles of 111.8˚ and 105.7˚, $r_{C=O}$ = 1.222 to 1.226 Å, r_{C-C} = 1.495 to 1.502 Å, and r_{Cu-O} = 2.088 to 2.109 Å. As expected, the r_{Cu-O} are longer than in Cu^+(Ace) and $Cu^+(Ace)(N_2)_2$, while the bonds in the acetone are less perturbed. The simulated vibrational spectrum is an excellent match to the experiment. The computed Cu-$\widehat{O}$-C angles in $Cu^+(Ace)_4$ are much smaller than in $Cu^{2+}(Ace)_4$ (~135°). The angle is likely due to compromise between charge transfer (which favors angles of 90°) and electrostatics (180°), with electrostatics having more influence in the 2+ complex.

Previously, we studied the interaction between Al^+ and acetones.[26] The acetones in $Cu^+(Ace)_4$ all directly coordinate to the metal, whereas in $Al^+(Ace)_4$, three acetones directly coordinate to Al^+ and one acetone is in the second solvation shell. The vibrational spectrum of $Al^+(Ace)_4$ contains two strong peaks in the C=O stretching region at 1672 (first shell acetones) and 1731 cm^{-1} (second shell acetone). Acetones in the first solvation shell of $Al^+(Ace)_4$ show a larger red shift in the C=O stretch than those in $Cu^+(Ace)_4$. Although the Al-O-C in computed Al^+(Ace) are collinear, this is not the case for the larger clusters. In computed $Al^+(Ace)_4$ the Al-$\widehat{O}$-C angles are 135.4 to 138.2°, which is similar to the values in computed $M^{2+}(Ace)_4$.

Our previous calculations showed that the most stable isomer for $Al^+(Ace)_n$ with n ≥ 3 is a pinacolate (Pin) produced by C–C reductive coupling of two adjacent acetones, along with formation of two Al-O covalent bonds and formal oxidation of the metal to the 3+ state. The experimental vibrational spectrum showed a characteristic pinacolate peak at 1185 cm^{-1} for n = 5. Therefore, for $Cu^+(Ace)_4$, we also considered a pinacolate isomer $Cu^+(Pin)(Ace)_2$. However, the calculation predicts that it lies 283.8 kJ/mol above $Cu^+(Ace)_4$. It is predicted to have a distinctive peak at 1144 cm^{-1}. This is not observed in the experiment, which is not surprising as it lies at very high energy, because a 3+ oxidation state is very unfavorable for copper.

Conclusions

The structure and bonding of $M^{+/2+}(Ace)_n$, M^+ = Cu, M^{2+} = Co, Ni, Cu, and Zn, n = 1 and 4, are examined using photodissociation vibrational spectroscopy and density functional theory calculations. The calculated vibrational spectra at the B3LYP+D3/6-311+G(d,p) level of theory match experiment better than those at the ωB97X–D/6-311+G(d,p) level. Interaction between the metal ion and acetone weakens the C=O bond and slightly strengthens the C-C bonds, which leads to a red shift in the C=O stretch and blue shift in the antisymmetric CC stretch. Comparing Cu^+ and Cu^{2+} with the same number of acetone ligands, the higher oxidation state leads to a much higher bond dissociation energy (BDE) and larger C=O red shift. The specific metal has very little effect on the C=O red shift in $M^{2+}(Ace)_4$, implying that in the dication complexes the red shift is primarily due to simple electrostatic interactions. The specific electron configuration does affect the structure of $M^{2+}(Ace)_4$ complexes: Co, Ni, and Zn are calculated to have distorted tetrahedral geometries; Cu has a square planar geometry. In most of the complexes, the metal does not bind along the C=O bond. The M-O-C bond is bent due to sdσ hybridization and charge transfer. Comparison of Cu^+(Ace) and $Cu^+(Ace)_4$ shows that the red shift of the C=O stretch decreases as the size of the cluster increases. There is no intramolecular C–C reductive coupling reaction observed for $Cu^+(Ace)_4$. In agreement with previous work by Zhang *et al*.,[51] the calculated red shift in the C=O stretch in $M^{+/2+}$(Ace) is correlated with the shift in the population of C=O antibonding orbitals upon acetone binding to the metal. However, there is a stronger correlation with a more fundamental property: the ionization energy of the metal. This correlation holds for a wide range of metal cations and dications, open- and closed-shell. Despite this correlation, Al^+ exhibits larger red shifts than expected.

Author Contributions

Apakorn Phasuk: Formal analysis (lead); Investigation (lead); Writing – original draft (lead); Writing – review & editing (supporting).

Ricardo B. Metz: Conceptualization (lead); Formal analysis (supporting); Funding acquisition (lead); Writing – original draft (supporting); Writing – review & editing (lead).

Joel Lemaire: Investigation (lead)

Vincent Steinmetz: Investigation (supporting)

Philippe Maître: Investigation (supporting), Resources (supporting)

Conflicts of interest

There are no conflicts to declare.

Acknowledgements

Financial support from the National Science Foundation under award no. CHE-2154391 is gratefully acknowledged. AP is supported by a Development and Promotion of Science and Technology Talents Project, Thai government scholarship. The authors are grateful for computational resources provided by the Massachusetts Green High-Performance Computing Center (MGHPCC).

References

1 J. J. Varghese and S. H. Mushrif, *React. Chem. Eng.*, 2019, **4**, 165–206.
2 P. J. Dyson and P. G. Jessop, *Catal. Sci. Technol.*, 2016, **6**, 3302–3316.
3 R. A. Rajadhyaksha and S. L. Karwa, *Chem. Eng. Sci.*, 1986, **41**, 1765–1770.
4 A. J. Stace, *Phys. Chem. Chem. Phys.*, 2001, **3**, 1935–1941.
5 C.-J. Li, *Chem. Rev.*, 2005, **105**, 3095–3165.
6 T. Hirao, *Top. Curr. Chem.*, 2007, **279**, 53–75.
7 R. D. Rieke and S. Kim, *J. Org. Chem.*, 1998, **63**, 5235–5239.
8 P. E. M. Siegbahn and M. R. A. Blomberg, *Chem. Rev.*, 2000, **100**, 421–437.
9 M. T. Rodgers and P. B. Armentrout, *Acc. Chem. Res.*, 2004, **37**, 989–998.
10 A. S. Lemoff, M. F. Bush, C. C. Wu and E. R. Williams, *J. Am. Chem. Soc.*, 2005, **127**, 10276–10286.
11 K. R. Asmis, *Phys. Chem. Chem. Phys.*, 2012, **14**, 9270–9281.
12 P. I. Surjasasmita and B. S. Freiser, *J. Am. Soc. Mass Spectrom.*, 1993, **4**, 135–144.
13 J. Wu, D. Liu, J. G. Zhou, F. Hagelberg, S. S. Park and A. A. Shvartsburg, *J. Phys. Chem. A*, 2007, **111**, 4748–4758.
14 M. J. Van Stipdonk, C. O'Malley, A. Plaviak, D. Martin, J. Pestok, P. A. Mihm, C. G. Hanley, T. A. Corcovilos, J. K. Gibson and B. J. Bythell, *Int. J. Mass Spectrom.*, 2016, **396**, 22–34.
15 R. R. Wright, N. R. Walker, S. Firth and A. J. Stace, *J. Phys. Chem. A*, 2001, **105**, 54–64.
16 B. J. Duncombe, L. Puškar, B. Wu and A. J. Stace, *Can. J. Chem.*, 2005, **83**, 1994–2004.
17 R. L. Jarek, T. D. Miles, M. L. Trester, S. C. Denson and S. K. Shin, *J. Phys. Chem. A*, 2000, **104**, 2230–2237.
18 Y. P. Ho, Y. C. Yang, S. J. Klippenstein and R. C. Dunbar, *J. Phys. Chem. A*, 1997, **101**, 3338–3347.
19 B. C. Guo, B. J. Conklin and A. W. Castleman Jr., *J. Am. Chem. Soc.*, 1989, **111**, 6506–6510.
20 Y. M. Koo, K. Hong, T. K. Kim and K. W. Jung, *Bull. Korean Chem. Soc.*, 2010, **31**, 953–958.
21 K. F. Willey, P. Y. Cheng, M. B. Bishop and M. A. Ducan, *J. Am. Chem. Soc.*, 1991, **113**, 4721–4728.
22 J. Roithová, *Chem. Soc. Rev.*, 2012, **41**, 547–559.
23 J. Velasquez, E. D. Pillai, P. D. Carnegie and M. A. Duncan, *J. Phys. Chem. A*, 2006, **110**, 2325–2330.
24 G. S. Groenewold, A. K. Gianotto, K. C. Cossel, M. J. Van Stipdonk, D. T. Moore, N. Polfer, J. Oomens, W. A. De Jong and L. Visscher, *J. Am. Chem. Soc.*, 2006, **128**, 4802–4813.
25 G. S. Groenewold, A. K. Gianotto, K. C. Cossel, M. J. Van Stipdonk, J. Oomens, N. Polfer, D. T. Moore, W. A. De Jong and M. E. McIlwain, *Phys. Chem. Chem. Phys.*, 2007, **9**, 596–606.
26 A. Phasuk and R. B. Metz, *J. Phys. Chem. Lett.*, 2023, **14**, 6295–6300.
27 J. Husband, F. Aguirre, P. Ferguson and R. B. Metz, *J. Chem. Phys.*, 1999, **111**, 1433–1437.
28 A. Kocak, G. Austein-Miller, W. L. Pearson, G. Altinay and R. B. Metz, *J. Phys. Chem. A*, 2013, **117**, 1254–1264.
29 D. Kaur, A. M. de Souza, J. Wanna, S. A. Hammad, L. Mercorelli and D. S. Perry, *Appl. Opt.*, 1990, **29**, 119–124.
30 I. E. Gordon, L. S. Rothman, C. Hill, R. V. Kochanov, Y. Tan, P. F. Bernath, M. Birk, V. Boudon, A. Campargue, K. V. Chance, B. J. Drouin, J. M. Flaud, R. R. Gamache, J. T. Hodges, D. Jacquemart, V. I. Perevalov, A. Perrin, K. P. Shine, M. A. H. Smith, J. Tennyson, G. C. Toon, H. Tran, V. G. Tyuterev, A. Barbe, A. G. Császár, V. M. Devi, T. Furtenbacher, J. J. Harrison, J. M. Hartmann, A. Jolly, T. J. Johnson, T. Karman, I. Kleiner, A. A. Kyuberis, J. Loos, O. M. Lyulin, S. T. Massie, S. N. Mikhailenko, N. Moazzen-Ahmadi, H. S. P. Müller, O. V. Naumenko, A. V. Nikitin, O. L. Polyansky, M. Rey, M. Rotger, S. W. Sharpe, K. Sung, E. Starikova, S. A. Tashkun, J. Vander Auwera, G. Wagner, J. Wilzewski, P. Wcisło, S. Yu and E. J. Zak, *J. Quant. Spectrosc. Radiat. Transf.*, 2017, **203**, 3–69.
31 L. MacAleese, A. Simon, T. B. McMahon, J. M. Ortega, D. Scuderi, J. Lemaire and P. Maître, *Int. J. Mass Spectrom.*, 2006, **249**–**250**, 14–20.
32 A. Simon, L. MacAleese, P. Maître, J. Lemaire and T. B. McMahon, *J. Am. Chem. Soc.*, 2007, **129**, 2829–2840.
33 L. MacAleese and P. Maître, *Mass Spectrom. Rev.*, 2007, **26**, 583–605.
34 R. Prazeres, F. Glotin, C. Insa, D. A. Jaroszynski and J. M. Ortega, *Eur. Phys. J. D*, 1998, **3**, 87–93.
35 M. J. Frisch, G. W. Trucks, H. B. Schlegel, G. E. Scuseria, M. a. Robb, J. R. Cheeseman, G. Scalmani, V. Barone, G. a. Petersson, H. Nakatsuji, X. Li, M. Caricato, a. V. Marenich, J. Bloino, B. G. Janesko, R. Gomperts, B. Mennucci, H. P. Hratchian, J. V. Ortiz, a. F. Izmaylov, J. L. Sonnenberg, Williams, F. Ding, F. Lipparini, F. Egidi, J. Goings, B. Peng, A. Petrone, T. Henderson, D. Ranasinghe, V. G. Zakrzewski, J.

Gao, N. Rega, G. Zheng, W. Liang, M. Hada, M. Ehara, K. Toyota, R. Fukuda, J. Hasegawa, M. Ishida, T. Nakajima, Y. Honda, O. Kitao, H. Nakai, T. Vreven, K. Throssell, J. a. Montgomery Jr., J. E. Peralta, F. Ogliaro, M. J. Bearpark, J. J. Heyd, E. N. Brothers, K. N. Kudin, V. N. Staroverov, T. a. Keith, R. Kobayashi, J. Normand, K. Raghavachari, a. P. Rendell, J. C. Burant, S. S. Iyengar, J. Tomasi, M. Cossi, J. M. Millam, M. Klene, C. Adamo, R. Cammi, J. W. Ochterski, R. L. Martin, K. Morokuma, O. Farkas, J. B. Foresman and D. J. Fox, 2013, Gaussian 09, Revision D.01, Gaussian, Inc.

36 S. Grimme, J. Antony, S. Ehrlich and H. Krieg, *J. Chem. Phys.*, 2010, **132**, 154104.

37 J.-D. Chai and M. Head-Gordon, *Phys. Chem. Chem. Phys.*, 2008, **10**, 6615–6620.

38 A. E. Reed, L. A. Curtiss and F. Weinhold, *Chem. Rev.*, 1988, **88**, 899–926.

39 L. Puškar and A. J. Stace, *Mol. Phys.*, 2005, **103**, 1829–1835.

40 Y. Chu, Z. Yang and M. T. Rodgers, *J. Am. Soc. Mass Spectrom.*, 2002, **13**, 453–468.

41 A. M. El-Nahas, *Chem. Phys. Lett.*, 2002, **365**, 251–259.

42 M. Peschke, A. T. Blades and P. Kebarle, *J. Am. Chem. Soc.*, 2000, **122**, 10440–10449.

43 C. W. Bauschlicher Jr., S. R. Langhoff and H. Partridge, *J. Chem. Phys.*, 1991, **94**, 2068–2072.

44 M. Peschke, A. T. Blades and P. Kebarle, *J. Am. Chem. Soc.*, 2000, **122**, 10440–10449.

45 J. Stanley-Gray, Z. Zhang and D. Venkataraman, *J. Chem. Educ.*, 2021, **98**, 2476–2481.

46 N. R. Walker, S. Firth and A. J. Stace, *Chem. Phys. Lett.*, 1998, **292**, 125–132.

47 A. M. Lamsabhi, M. Yáñez, J.-Y. Salpin and J. Tortajada, in *Patai's Chemistry of Functional Groups*, Wiley, 2011.

48 J. Guan, L. Puškar, R. O. Esplugas, H. Cox and A. J. Stace, *J. Chem. Phys.*, 2007, **127**, 064311.

49 T. Shimanouchi, *Tables of Molecular Vibrational Frequencies, Consolidated Volume I*, National Bureau of Standards, Gaithersburg, MD, 1972.

50 F. Bouchard, V. Brenner, C. Carra, J. W. Hepburn, G. K. Koyanagi, T. B. McMahon, G. Ohanessian and M. Peschke, *J. Phys. Chem. A*, 1997, **101**, 5885–5894.

51 G. Zhang, W. Wang and D. Chen, *Chem. Phys.*, 2009, **359**, 40–44.

52 M. Rahm, R. Hoffmann and N. W. Ashcroft, *Chem. – A Eur. J.*, 2016, **22**, 14625–14632.

53 D. P. Duda and D. A. Dixon, *J. Phys. Chem. A*, 2023, **127**, 9985–9994.

